



# Cyanobacteria–probiotics symbionts for modulation of intestinal inflammation and microbiome dysregulation in colitis

Jiali Yang<sup>a,b,1</sup>, Shaochong Tan<sup>a,1</sup>, Shengchan Ge<sup>a</sup>, Mingzhu Yang<sup>a</sup>, Hua Liu<sup>a</sup>, Wei Liu<sup>a</sup> , Kaixiang Zhang<sup>a</sup> , Zhenzhong Zhang<sup>a,c,2</sup>, Zhi-Hao Wang<sup>a,2</sup> , Jinjin Shi<sup>a,c,d,2</sup> , and Junjie Liu<sup>a,2</sup>

Edited by Chun-jun Guo, Weill Cornell Medicine, New York, NY; received February 18, 2024; accepted November 5, 2024 by

Editorial Board Member Carl F. Nathan

Inflammatory bowel disease (IBD) is often associated with excessive inflammatory response and highly dysregulated gut microbiota. Traditional treatments utilize drugs to manage inflammation, potentially with probiotic therapy as an adjuvant. However, current standard practices often suffer from detrimental side effects, low bioavailability, and unsatisfactory therapeutic outcomes. Microbial complexes characterized by mutually beneficial symbiosis hold great promise for IBD therapy. Here, we aggregated *Synechocystis* sp. PCC6803 (Sp) with *Bacillus subtilis* (BS) by biomimetic mineralization to form cyanobacteria–probiotics symbionts (ASp@BS), which reshaped a healthy immune system and gut microbiota in a murine model of acute colitis. The symbionts exhibited excellent tolerance to the harsh environment of the gastrointestinal tract. Importantly, probiotics within the symbionts created a local anaerobic environment to activate the [NiFe]-hydrogenase enzyme of cyanobacteria, facilitating the production of hydrogen gas (H<sub>2</sub>) to persistently scavenge elevated reactive oxygen species and alleviate inflammatory factors. The resulting reduced inflammation improves the viability of the probiotics to efficiently regulate the gut microbiota and reshape the intestinal barrier functions. Our research elucidates that ASp@BS leverages the synergistic interaction between Sp and BS to create a therapeutic platform that addresses multiple aspects of IBD, offering a promising and comprehensive solution for IBD treatment.

inflammatory bowel disease | cyanobacteria-probiotics symbionts | hydrogen gas | gut microbiota

Inflammatory bowel disease (IBD) comprises a family of idiopathic gastrointestinal disorders that includes Crohn's disease (CD) and ulcerative colitis (UC), which can lead to more serious diseases such as colorectal cancer (1–3). Although the pathogenesis of IBD is complex and elusive, emerging evidence suggests that IBD is associated with intestinal mucosal barrier dysfunction and dysbiosis of the gut microbiota, which subsequently leads to an overactive immune response and inflammatory factors with elevated reactive oxygen species (ROS) (4). Currently available clinical therapies for IBD primarily focus on improving disease-related symptoms by either reducing the burden of intestinal inflammation or suppressing the immune response (5). These therapies include drugs such as 5-aminosalicylates (5-ASA), corticosteroids, and tumor necrosis factor (TNF) antagonists (5, 6). However, these treatments often fail to address the root causes of IBD, which include damage to the gastrointestinal mucosal layer, loss of intestinal barrier function, and dysregulation of the gut microbiota. Furthermore, traditional immunosuppressive agents based on small molecules or biologics can result in off-target systemic side effects and may lead to serious complications with prolonged use, including opportunistic infections, malignancies, autoimmune conditions, and liver toxicity (1, 7–9). Recent studies have shown that the microbiome plays a crucial role in regulating essential immune functions in both health and various disease contexts, including IBD (10). The emerging understanding of the microbiome's role in the pathogenesis of the disease and the anti-inflammatory properties of certain symbiotic microorganisms support the use of probiotic-based therapies for IBD (11–13). Oral probiotic therapy has shown promise as an adjunctive treatment for IBD by enabling the balance of bacterial composition in the intestines to be actively modulated and promoting mucosal healing (14, 15). However, oral administration of probiotics has been limited by their low bioavailability—given these probiotics are susceptible to ROS damage in the context of IBD—reducing treatment efficacy and prolonging therapy duration (16–18). There is an unmet need for more effective and safer IBD therapies targeting suppression of inflammation, reestablishment of intestinal barrier function, and modulation of the gut microbiota in infected tissues.

Symbiotic relationships between microorganisms play a fundamental role in ecosystem processes and evolutionary pathways (19). Importantly, microbial complexes characterized by mutually beneficial symbiosis hold great promise for disease therapy (20–22). Microorganisms

## Significance

The present symbionts exhibited excellent tolerance to the harsh environment of the gastrointestinal tract. Importantly, probiotics within symbionts created a local anaerobic environment to activate the [NiFe]-hydrogenase enzyme of cyanobacteria, facilitating the production of hydrogen gas to persistently scavenge elevated reactive oxygen species and alleviate inflammatory factors. The reduced inflammation caused by cyanobacteria improves the viability of the probiotics to efficiently regulate gut microbiota homeostasis and reshape the intestinal barrier function.

Author affiliations: <sup>a</sup>Department of Pharmaceutical Analysis, School of Pharmaceutical Sciences, Zhengzhou University, Zhengzhou 450001, People's Republic of China; <sup>b</sup>Department of Neuroscience, Institute of Brain Science and Disease, Qingdao Medical College of Qingdao University, Shandong Provincial Key Laboratory of Pathogenesis and Prevention of Neurological Disorders, Qingdao University, Qingdao 266021, People's Republic of China; <sup>c</sup>Key Laboratory of Targeting Therapy and Diagnosis for Critical Diseases, Zhengzhou 450001, People's Republic of China; and <sup>d</sup>State Key Laboratory of Esophageal Cancer Prevention and Treatment, Zhengzhou 450001, People's Republic of China

Author contributions: J.Y., Z.Z., J.S., and J.L. designed research; J.Y., S.T., S.G., M.Y., and H.L. performed research; W.L., K.Z., and Z.-H.W. analyzed data; and J.Y. and J.L. wrote the paper.

The authors declare no competing interest.

This article is a PNAS Direct Submission. C.-j.G. is a guest editor invited by the Editorial Board.

Copyright © 2024 the Author(s). Published by PNAS. This article is distributed under [Creative Commons Attribution-NonCommercial-NoDerivatives License 4.0 \(CC BY-NC-ND\)](https://creativecommons.org/licenses/by-nc-nd/4.0/).

<sup>1</sup>J.Y. and S.T. contributed equally to this work.

<sup>2</sup>To whom correspondence may be addressed. Email: zhangzhenzhong@zzu.edu.cn, wangzhihao@zzu.edu.cn, shijinyx@zzu.edu.cn, or liujunjie@zzu.edu.cn.

This article contains supporting information online at <https://www.pnas.org/lookup/suppl/doi:10.1073/pnas.2403417121/-/DCSupplemental>.

Published December 16, 2024.

with symbiotic relationships can synergistically exert functions that cannot be achieved by a single microorganism, thereby increasing the efficiency of microbiome-based biotherapies (3, 23). *Synechocystis* sp. PCC6803 (Sp) is a cyanobacterium that can produce hydrogen through dark fermentation under anaerobic conditions (24–26). However, the [NiFe]-hydrogenase (HoxEFUYH) in Sp is oxygen-sensitive, with its hydrogen-producing capabilities being limited by local oxygen concentrations (24–26). *Bacillus subtilis* (BS) is a probiotic renowned for its ability to rapidly consume free oxygen (27) and inhibit the growth of pathogenic bacteria (28–30). However, the therapeutic potential of BS is often limited by excessive oxidative conditions within the gastrointestinal tract in the pathological context. IBD is typically accompanied by a hyperoxic and highly oxidative microenvironment (31), which limits the therapeutic efficacy of Sp and BS when each is used independently.

Given the above limitations of using these strains individually, in this study, cyanobacterial-probiotic symbionts were established for the effective treatment of IBD. Specifically, we used a biomimetic mineralization process to aggregate the cyanobacterium Sp with the probiotic BS to form a symbiont (ASp@BS). In this symbiotic system, BS can consume oxygen to create a local anaerobic environment, which activates [NiFe]-hydrogenase of cyanobacteria to promote H<sub>2</sub> production, initiating antioxidant and anti-inflammatory responses. In a mutually beneficial relationship, H<sub>2</sub> produced by cyanobacteria persistently eliminates ROS (32, 33), exerting a powerful protective effect on the probiotics against oxidative damage under these inflammatory conditions, thereby remodeling the gut barrier function and gut microbiota. Additionally, the symbiotic aggregate is not affected by harsh gastrointestinal conditions, including the presence of gastric acid and bile salts, which enhances the efficiency of oral delivery. The research results highlight the ability of the ASp@BS system to alleviate inflammatory symptoms, regulate the gut microbiota, and restore intestinal barrier function, ultimately producing a potent therapeutic effect in a DSS-induced acute colitis model. In summary, the present ASp@BS symbiont, utilizing the synergy between Sp and BS, represents a therapeutic platform that not only substitutes clinical anti-inflammatory drugs but also shields probiotics from adverse stressors. This symbiont addresses multiple facets of IBD, offering a promising comprehensive solution for its treatment.

## Results

**Intermicroorganism Mutualism between Sp and BS Holds the Potential to Treat IBD.** IBD is often associated with an overactive inflammatory response and highly dysregulated gut microbiota (4, 6, 8, 34). As an excellent antioxidant and anti-inflammatory agent, H<sub>2</sub> can be used for treating IBDs (35–37). Furthermore, probiotics have beneficial functions in regulating gut microbiota. Therefore, we hypothesized that the symbiosis of Sp and BS could effectively treat IBD (Fig. 1A). To validate this hypothesis, we first measured the oxygen concentration in the symbiotic system. When Sp and BS were cocultured, the O<sub>2</sub> concentration in the system gradually decreased with time, and the O<sub>2</sub> concentration was almost zero after 8 h (Fig. 1B). Then, a simple apparatus was designed to collect the generated H<sub>2</sub> (Fig. 1C), inject it into a gas chromatograph (GC), and perform quantification (Fig. 1D). The coculture of Sp and BS produced 8.6 μmol of H<sub>2</sub>, and neither Sp nor BS alone produced H<sub>2</sub>. Furthermore, hydrogenase activity was quantified based on the hydrogen production rate, which was significantly higher for the coculture of Sp and BS than for Sp alone (SI Appendix, Fig. S1). A methyl blue-platinum (MB-Pt) probe (38) was used to further investigate the H<sub>2</sub>-producing ability of Sp+BS. In the presence of a platinum catalyst, MB was reduced by H<sub>2</sub> (Fig. 1E). Upon addition of

the Sp+BS suspension once H<sub>2</sub> production had been completed, the characteristic peak of the MB probe at 664 nm decreased significantly and the color of MB gradually faded (Fig. 1F). These results indicated that BS is able to consume oxygen, causing a localized anaerobic microenvironment which in turn activates [NiFe]-hydrogenase in Sp, promoting H<sub>2</sub> production.

Based on the effective H<sub>2</sub> production behavior of the coculture, we investigated the ability to scavenge reactive oxygen species (ROS) of Sp and BS in vitro. The ABTS method was utilized to assess the coculture of Sp and BS ability to clear hydroxyl radicals (•OH). Compared with BS and Sp, the coculture of BS and ASp was the most efficient in reducing •OH, with a clearance efficiency of 58.1% (Fig. 1G and H). The protective effect on probiotics under high oxidative stress was further investigated. After treating the cocultures in hydrogen peroxide (H<sub>2</sub>O<sub>2</sub>), the survival rate of bacteria in the Sp and BS coculture was significantly increased by 5.3 folds compared with that when BS was cultured alone (Fig. 1I). The above results confirm that the symbiotic properties of Sp and BS have great potential for the treatment of IBD.

**Preparation and Characterization of ASp@BS.** In order to ensure that the mutually beneficial symbiotic relationship between Sp and BS was still functional in vivo, we synthesized cyanobacterial-probiotic symbionts (ASp@BS) via a one-step synthesis using the biomimetic mineralization method (39) (Fig. 2A). Specifically, we first introduced polydiallyldimethylammonium chloride (PDADMAC) onto the surface of Sp cells. PDADMAC molecules can interact with Sp cells and modify their properties, creating a biomimetic silicified protein layer. PDADMAC is a cationic polymer containing quaternary amines to simulate silicification proteins and successfully encapsulate individual cells with silica (40). This technique has proven successful in conferring cyanobacteria aggregates with characteristics akin to those of diatoms (39, 41). Next, the modified cells were resuspended in a sodium silicate solution, inducing spontaneous aggregation behavior. During this aggregation process, by adding the probiotic BS, we effectively encapsulated BS within the aggregates. Determination of the optimal ratio of Sp and BS was pivotal. We synthesized ASp@BS with different ratios and then observed the aggregation of BS and Sp cells by confocal laser scanning microscopy (CLSM). As shown in SI Appendix, Fig. S2, BS concentration of 1 × 10<sup>8</sup> CFU/mL combined with 3 × 10<sup>8</sup> Sp cells/mL, provided the optimal ratio, producing aggregates with the highest BS load while maintaining structural integrity. Dynamic light scattering (DLS) results revealed that the surface potential of Sp cells was approximately -26.8 ± 0.23 mV. After modifying the algae surface with PDADMAC, the surface potential shifted to 15.5 ± 0.47 mV. Subsequent mineralization resulted in ASp@BS with a surface potential shift to -3.3 ± 0.4 mV, thereby confirming the formation of ASp@BS through the observed changes in potential (Fig. 2B). Subsequently, we employed scanning electron microscopy (SEM) to characterize the surface morphology of ASp@BS. The SEM results depicted aggregate sizes of around 100 μm, and zoomed-in images revealed the close interconnection of numerous algae and bacteria within the aggregates (Fig. 2C and D). Further observation using CLSM demonstrated the successful colocalization of green fluorescent protein (GFP) from the bacteria and red fluorescence (chlorophyll a, phycocyanin) from the algae (Fig. 2E). Moreover, the CLSM 3D images also confirmed the successful synthesis of ASp@BS (Fig. 2F). Additionally, infrared spectroscopy and energy dispersive X-ray spectroscopy (EDS) analysis indicated self-aggregation achieved by the interbonding of individual algae cells through amorphous silica on their surfaces (Fig. 2G and SI Appendix, Figs. S3 and S4).

Oral administration is the preferred method of drug delivery for the treatment of chronic gastrointestinal disorders owing to

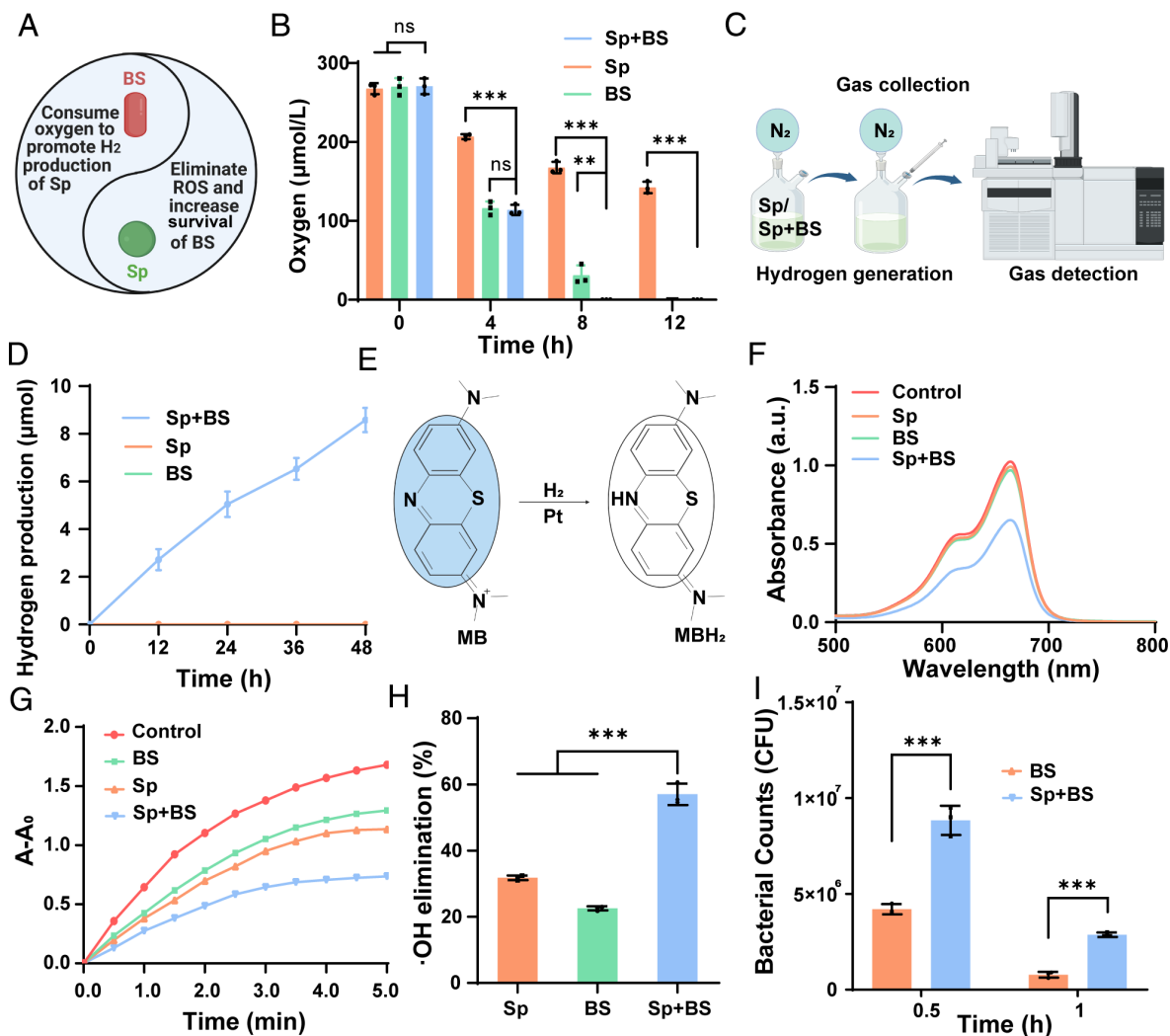


**Fig. 1.** Intermicroorganism mutualism between Sp and BS holds the potential to treat IBD. (A) Schematic representation of intermicroorganism mutualism between Sp and BS. (B) The O<sub>2</sub> concentration in the Sp and BS coculture system. (C) Schematic diagram of a simple apparatus for H<sub>2</sub> collection and quantitative measurement. (D) Accumulated amount of H<sub>2</sub> produced by various suspensions, quantified by gas chromatography. (E) Reaction equation of H<sub>2</sub> and MB-Pt reagent (H<sub>2</sub>-detecting probe). The *Inset* shows the molecular structure change of MB after H<sub>2</sub> reduction. (F) MB-platinum was incubated in different suspensions and the UV-vis absorption spectra were measured. (G and H) •OH-scavenging ability of different suspensions measured by ABTS method. (I) The survival of the BS was evaluated in the presence of 200 μM of H<sub>2</sub>O<sub>2</sub>. Data are presented as the mean ± SD (n = 3); \*P < 0.05, \*\*P < 0.01, and \*\*\*P < 0.001 determined by Student's t test.

its convenience, safety, and direct action on the local mucosa. However, orally administered agents encounter a hostile environment in the gastrointestinal tract. To evaluate the resistance of ASp@BS to the gastrointestinal environment after oral administration, experiments were conducted. As illustrated in Fig. 2H, ASp@BS maintained its structural integrity even after exposure to simulated gastric fluid (SGF) for 2 h, bile salts for 6 h, and simulated colonic fluid (SCF) for 6 h, demonstrating that it is stable in the gastrointestinal tract (Fig. 2H and *SI Appendix*, Fig. S5). Similarly, colocalization of Sp and BS was still observed in intestinal sections 48 h after oral administration of ASp@BS, indicating the stability of the ASp@BS oral delivery platform (Fig. 2I). Furthermore, the growth curve and CCK8 assay results demonstrated the excellent biocompatibility of this synthesis method (*SI Appendix*, Figs. S6 and S7).

**H<sub>2</sub> Generation and ROS Elimination Ability of ASp@BS.** Next, we investigated whether ASp@BS could maintain a mutually beneficial symbiotic relationship between Sp and BS (Fig. 3A). As shown in Fig. 3B, ASp@BS produced 13.8 μmol of H<sub>2</sub> in 48 h. Aggregates without BS (ASp) also produced 2.5 μmol of H<sub>2</sub>, possibly due to anaerobic microenvironments created by oxygen

consumption during cellular respiration inside the ASp under dark conditions. The MB probe similarly confirmed that ASp@BS produced more H<sub>2</sub> than ASp (Fig. 3C). It is noteworthy that ASp@BS could retain the ability to continuously produce H<sub>2</sub> even after treatment with stomach acid and bile salt (*SI Appendix*, Fig. S8). The ABTS method was utilized to assess the ability of ASp@BS to clear •OH. The ASp@BS suspension that had already produced H<sub>2</sub> demonstrated the highest efficiency in reducing •OH generation relative to ASp, with a clearance efficiency of 75.1% (Fig. 3D and E). Owing to its sustained H<sub>2</sub> production ability and efficient diffusion of H<sub>2</sub>, ASp@BS exhibited potential as an antioxidant, countering intracellular oxidative stress (Fig. 3F). To determine the effect of the H<sub>2</sub> produced by the algae-probiotics aggregates on the intracellular ROS level of CT26 cells, we induced the production of ROS by the H<sub>2</sub>O<sub>2</sub>. As shown in Fig. 3G, preincubation of cells with ASp@BS under dark conditions led to a reduction in intracellular ROS, indicating that ASp@BS can effectively defend against oxidative stress by generating H<sub>2</sub>. Similar trends were observed through flow cytometry analysis, which showed that the oxidation level of cells decreased from 61.5 to 19.6% (*SI Appendix*, Fig. S9). These results suggest that the aggregates can promote the formation of localized anaerobic microenvironments,

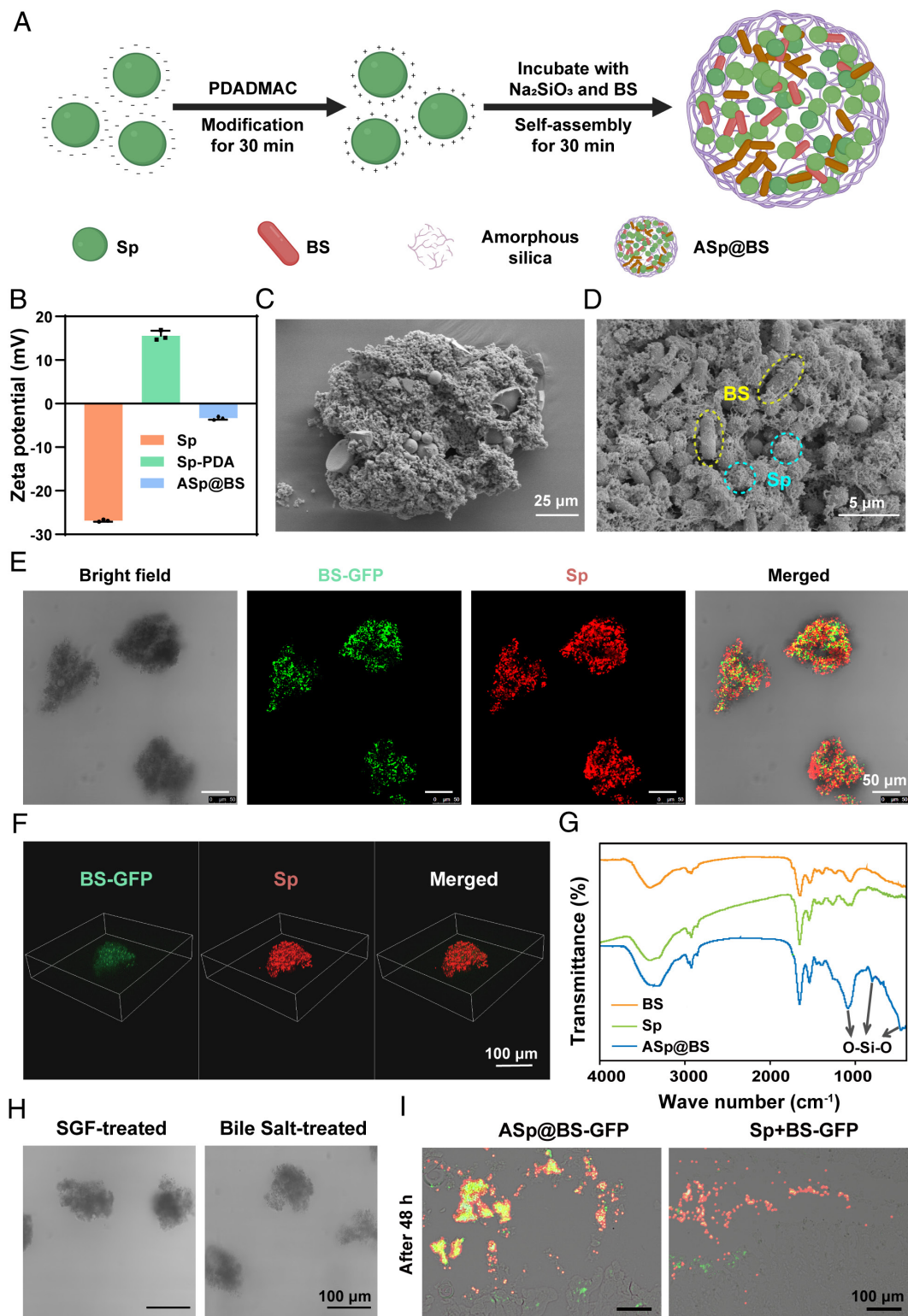


**Fig. 2.** Preparation, characterization, and assessment of stability of ASp@BS. (A) Schematic of the synthesis of ASp@BS. (B) Zeta potential of Sp, Sp-PDA, and ASp@BS ( $n = 3$ ). (C and D) Representative SEM image of ASp@BS and enlarged image. (E and F) Confocal fluorescence images of ASp@BS. The red fluorescence shows Sp and the green fluorescence shows BS-GFP. (G) FTIR of Sp, BS, and ASp@BS. (H) Representative fluorescence microscopy images of ASp@BS after reacting with SGF for 2 h and then bile salt for 6 h. (I) Representative fluorescence microscopy images of mouse colon collected at 48 h after oral gavage with BS+Sp or ASp@BS; GFP-expressing BS was used.

thereby activating hydrogenase within the Sp cells and producing H<sub>2</sub>. Furthermore, the potential of ASp@BS to generate H<sub>2</sub> in the intestine was also investigated. Ultrasound imaging confirmed that mice treated with ASp@BS exhibited a 2.5-fold increase in ultrasound signals, indicating the production of gas bubbles in

their abdomen (Fig. 3 H and I). These results confirmed that ASp@BS retained the symbiotic properties of the two microorganisms for effective H<sub>2</sub> production by Sp, with potent ROS scavenging capacity and the ability to protect cells from oxidative stress, exhibiting promise for the treatment of inflammation.

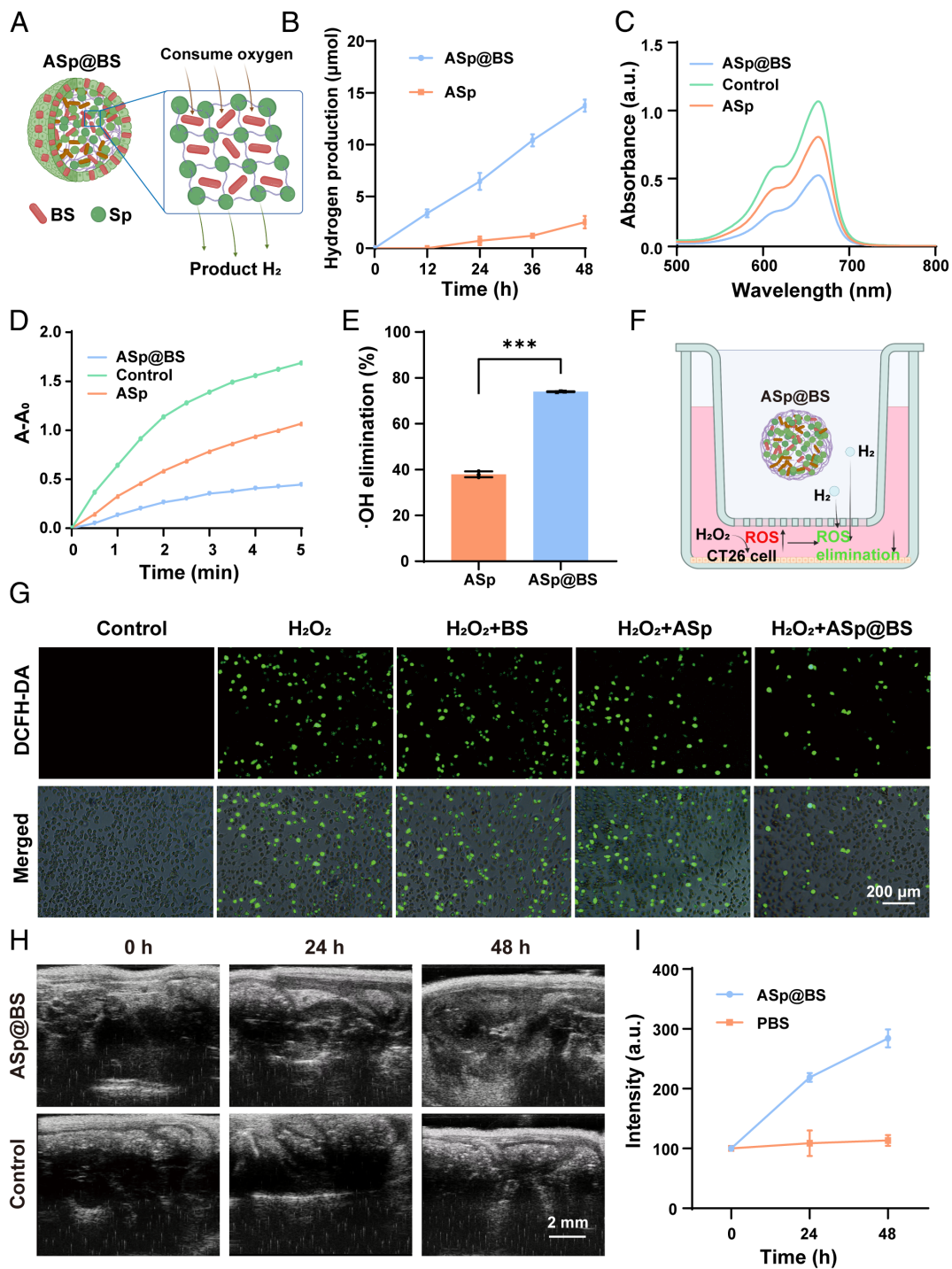


**Fig. 3.** H<sub>2</sub> generation and ROS elimination ability of Asp@BS. (A) Diagram of the mechanism of H<sub>2</sub> production by Asp@BS. (B) Accumulated amount of H<sub>2</sub> produced by various suspensions, quantified by gas chromatography. (C) MB-platinum was incubated in different suspensions and the UV-vis absorption spectra were measured. (D and E) ·OH-scavenging ability of different suspensions measured by ABTS method. (F) Schematic representation of the ability of different groups to scavenge ROS at the cellular level. (G) Confocal fluorescence images of ROS levels in CT26 cells after different treatments. Cells were stained with the ROS probe DCFH-DA (green fluorescence). (H) In vivo time-dependent ultrasound imaging of mice after oral administration of Asp@BS. (I) Quantitative analysis of signal intensities based on ultrasonic imaging data. Data are presented as the mean ± SD (n = 3); \*P < 0.05, \*\*P < 0.01, and \*\*\*P < 0.001, determined by Student's *t* test.

### Protection and Colonization of Probiotic Bacteria by Asp@BS.

Encouraged by the effective promotion of H<sub>2</sub> production by Sp in Asp@BS, we further explored the ability of Sp to exert protective effects on BS and promote its colonization. The protective effect of aggregates on BS probiotics was investigated through colony counting. When treated to SGF, BS inside aggregates exhibited superior vitality compared with unencapsulated BS, across different incubation intervals (*SI Appendix, Fig. S10A*). Remarkably, after 2 h, Asp@BS retained over  $1 \times 10^6$  viable bacteria, whereas

unencapsulated BS experienced near-complete bacterial death. Similarly, Asp@BS displayed enhanced viability in the presence of bile salts, indicating the protective role of the encapsulating layer against external stressors (*SI Appendix, Fig. S10B*). Further examination focused on the protective effect of Asp@BS on bacteria under high oxidative stress conditions. After subjecting the symbionts to H<sub>2</sub>O<sub>2</sub> treatment for 2 h, compared with BS, Asp@BS significantly improved the bacterial viability by 10.3 folds (*SI Appendix, Fig. S11*).

To investigate the *in vivo* adhesion and colonization capability of ASp@BS, mice were orally administered equal amounts of ASp@BS and BS. Bacterial colony counting was performed on harvested stomach and intestinal tissues at various time points (4, 48, and 96 h postadministration). The results showed that compared with the unmodified BS group, significantly higher quantities of bacteria of the ASp@BS group were found in both the stomach and intestine at all indicated time points (Fig. 4 *A–D*). After 4 h, the viable bacterial count of the ASp@BS group in the stomach was 7.9 times that of the natural BS group, demonstrating the tolerance of ASp@BS to gastric acid. Similarly, after 48 h of gavage, the number of bacteria in the intestines of the ASp@BS group was 4.6 times that in the intestines of the BS group. Even when the administration time was extended to 96 h, the colonization of bacteria in the intestine of the ASp@BS group was still 12.7 times higher than that in the BS group. To visually assess bacterial adhesion and colonization in the gastrointestinal tract, mice were orally administered equal amounts of ASp@BS-GFP and BS-GFP, and stomach and intestinal tissues were collected for IVIS imaging at designated time points. As shown in Fig. 4 *E* and *F*, the fluorescence intensity of the ASp@BS group was significantly higher than that of the BS group, indicating that ASp@BS enhances bacterial adhesion and colonization in mice. We also investigated the time-dependent distribution of ASp@BS in the gastrointestinal tract by detecting silicon in ASp@BS using inductively coupled plasma mass spectrometry (ICP-MS). As shown in *SI Appendix*, Fig. S12, after oral administration, ASp@BS primarily accumulated in the stomach within the first 2 h and gradually transitioned to the intestines over time. Notably, the highest cumulative concentrations were observed in the small intestine and colon at 8 and 12 h, respectively. Silica was still detected in the colon at 48 h, indicating that ASp@BS has an intestinal distribution time of more than 48 h. Additionally, ASp@BS was not detected in the blood or major organs, suggesting that ASp@BS is not readily transferred into the systemic circulation (*SI Appendix*, Figs. S12 and S13). Subsequently, the long-term adhesion and retention capabilities of ASp@BS were evaluated using CLSM. After oral administration of ASp@BS-GFP and BS-GFP, mice were killed on the third and sixth days, and colonic tissues were collected for frozen sections. As shown in Fig. 4*G*, the green fluorescence intensity of the ASp@BS group was significantly higher than that of the BS group, further confirming enhanced bacterial survival *in vivo*. Moreover, on the sixth day, green fluorescence was still observable in the ASp@BS group, while no fluorescence was detected in the BS group, indicating the prolonged retention of bacteria in the ASp@BS group. Importantly, comprehensive evaluation through measurement of body weight, complete blood count, blood biochemical indices, and hematoxylin-eosin (H&E) staining confirmed that administration of ASp@BS did not induce detectable damage or inflammatory reactions (*SI Appendix*, Figs. S14 and S15). In addition, we measured the levels of cytokines such as tumor necrosis factor- $\alpha$  (TNF- $\alpha$ ), interleukin-6 (IL-6), and interferon- $\gamma$  (IFN- $\gamma$ ) in the intestines of ASp@BS-treated mice. As shown in *SI Appendix*, Fig. S16, similar to that in the control group, no inflammatory response was seen in the ASp@BS group. In summary, the ASp@BS symbionts leverage the synergistic interaction between Sp and BS to create a therapeutic platform that addresses multiple aspects of IBD, offering a promising and comprehensive solution for IBD treatment.

**ASp@BS Ameliorate DSS-Induced Colitis.** Next, the therapeutic effect of ASp@BS on colitis *in vivo* was evaluated. Mice were administered ASp@BS, Sp+BS (BS mixed with Sp), BS, Sp, and SiO<sub>2</sub> for five consecutive days following a 7-d induction of colitis

using dextran sulfate sodium (DSS) (Fig. 5*A*). The experimental design included positive control mice treated with PBS and negative control mice not exposed to DSS. To gauge the impact of ASp@BS on colitis, changes in body weight were closely monitored. Although all mice exhibited weight loss after DSS induction, those treated with ASp@BS showed significantly less weight loss on the 13th day, indicating potent therapeutic effects against colitis (Fig. 5*B* and *SI Appendix*, Fig. S17*A*). Given that colitis-induced inflammation can lead to a shortened colon length, colonic tissues were isolated and measured to quantify colonic damage. The results demonstrated that, compared with the control group, mice treated with ASp@BS, Sp+BS, BS, Sp, SiO<sub>2</sub>, and PBS exhibited average reductions in colon length of 7.63%, 18.83%, 19.59%, 22.1%, 30.79%, and 37.4%, respectively (Fig. 5*C* and *SI Appendix*, Fig. S17 *C* and *D*). This confirmed the protective role of ASp@BS against colitis-induced damage. Additionally, the disease activity index score further underscored the substantial therapeutic effect of ASp@BS on colitis (Fig. 5*D* and *SI Appendix*, Fig. S17*B*).

Histological analysis was employed to evaluate the degree of colonic damage. Representative images showed that in the DSS group, the colonic structure was significantly disrupted, with lost crypts, depleted goblet cells, and immune cell infiltration. In contrast, treatment groups, especially the ASp@BS group, displayed notable improvements with nearly intact epithelial layers and minimal inflammatory cell infiltration (Fig. 5*E* and *SI Appendix*, Fig. S18*A*). Further, the apoptotic rate of colonic epithelial cells was assessed using a terminal deoxynucleotidyl transferase dUTP nick-end labeling (TUNEL) assay (42). The results revealed significantly fewer positive cells in the ASp@BS group than in other groups, signifying the ability of ASp@BS to reduce apoptosis of colonic epithelial cells (*SI Appendix*, Fig. S19). Next, the anti-inflammatory properties of ASp@BS were examined. Assessment of ROS levels in colonic tissues using DCF fluorescence imaging revealed that ASp@BS exhibited significantly better ROS-clearing effects *in vivo* than Sp+BS and BS. This result indicated that ASp@BS has the capability to produce higher levels of H<sub>2</sub> within the body, leading to robust ROS-clearing abilities (Fig. 5*F* and *SI Appendix*, Fig. S18*B*). To gauge the extent of neutrophil infiltration in colonic tissues, the activity of myeloperoxidase (MPO), a marker of neutrophil activity, was measured. The results showed that MPO activity in the ASp@BS group was notably lower than in all other treatment groups, demonstrating the strong anti-inflammatory effects of ASp@BS (*SI Appendix*, Fig. S20). The impact of ASp@BS on the inflammatory colonic epithelium and disruption of intestinal barrier function caused by DSS was also examined. Alcian blue/periodic acid–Schiff (AB/PAS) staining images also revealed that ASp@BS treatment significantly restored the mucus layer, similar to that in the healthy group (Fig. 5*G*). Administration of ASp@BS to DSS-induced colitis mice normalized the expression pattern of tight junction proteins ZO-1 and occludin in colonic tissues (Fig. 5*H* and *SI Appendix*, Fig. S18 *C* and *D*). These proteins play vital roles in maintaining intestinal homeostasis. This effect was minor in other control groups, including those that received Sp+BS and BS treatment. Furthermore, compared with other treatment approaches, ASp@BS effectively prevented systemic exposure to fluorescein isothiocyanate-dextran (FITC-dextran) upon oral administration in mice with colitis, indicating successful restoration of intestinal barrier function (*SI Appendix*, Fig. S21). The enzyme-linked immunosorbent assay was performed to quantify cytokine levels in colonic tissues. ASp@BS was found to reduce the levels of proinflammatory cytokines such as IL-6, interferon- $\gamma$ , and TNF- $\alpha$  while increasing the expression of anti-inflammatory cytokines such as IL-10 and

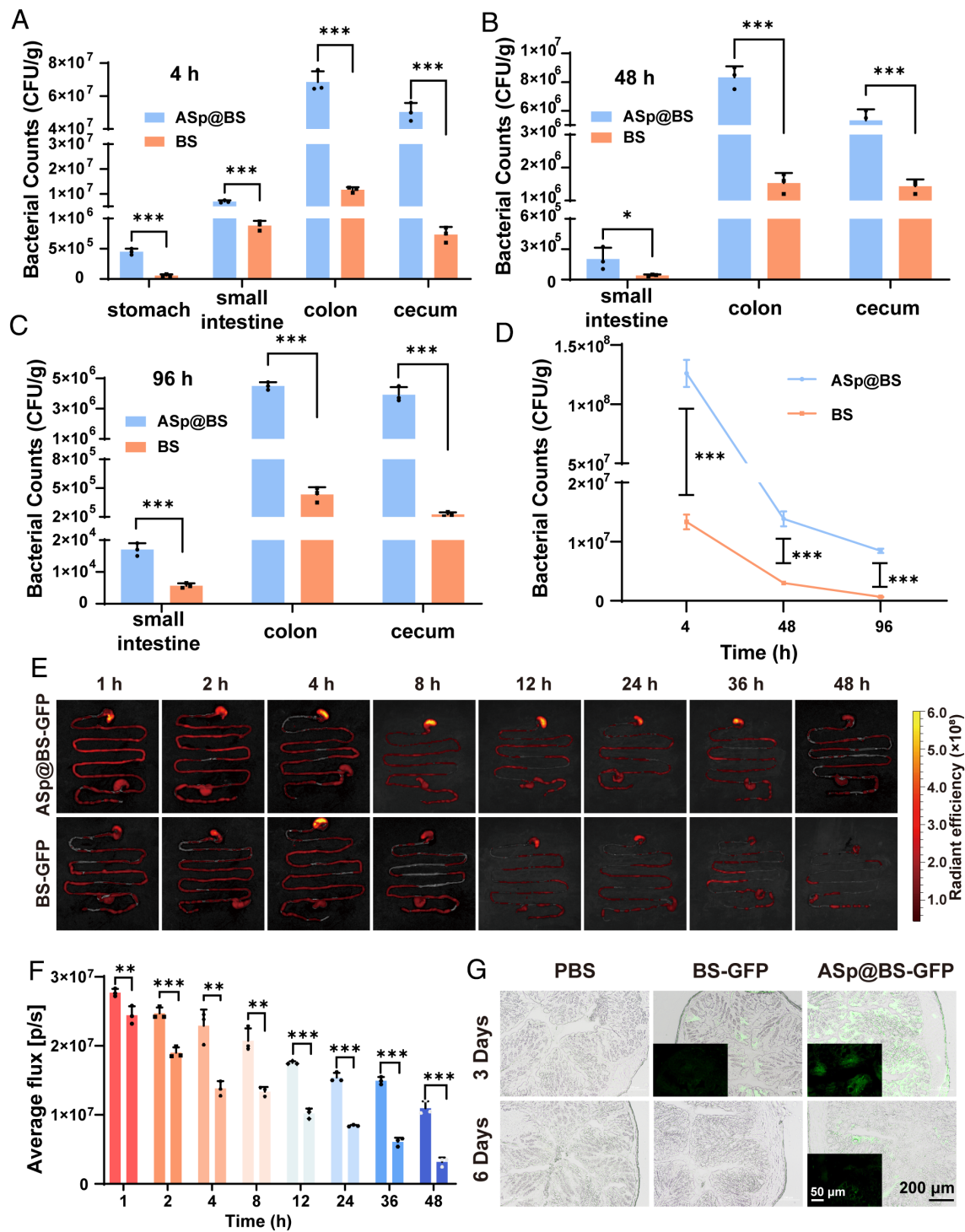


**Fig. 4.** Protection and colonization of probiotic bacteria by ASP@BS. (A–C) Counts of bacteria collected from the stomach, small intestine, colon, and cecum at 4, 48, and 96 h after oral gavage BS or ASP@BS. (D) Total counts of bacteria collected from the gastrointestinal tract at 4, 48, and 96 h after oral gavage BS or ASP@BS. (E and F) Representative IVIS images (E) and intensity (F) of GFP signals with the intestinal tracts after oral gavage of BS or ASP@BS. (G) Representative fluorescence microscopy images of mouse colon collected at 72 h and 144 h after oral gavage with PBS, BS, or ASP@BS; GFP-expressing BS were used. Data are presented as the mean  $\pm$  SD ( $n = 3$ ); \* $P < 0.05$ , \*\* $P < 0.01$ , and \*\*\* $P < 0.001$  determined by Student's *t* test.

TGF- $\beta$  (Fig. 5J). This balance between proinflammatory and anti-inflammatory cytokines further underscored the potent anti-inflammatory potential of ASP@BS.

To evaluate the preventive effect of ASP@BS on colitis in vivo, a DSS-induced mouse colitis prevention model was established, and different formulations of treatment were administered (SI Appendix, Fig. S22A). Consistent with previous results, ASP@BS demonstrated superior inhibition of colitis progression

compared with all other treatment groups, with reduced weight loss, longer colon length, and minimal colonic damage (SI Appendix, Fig. S22B–E). Taken together, these results provide comprehensive evidence of the potential of ASP@BS as a therapeutic option for colitis, which is attributable to its anti-inflammatory properties, ROS-clearing abilities, and restoration of intestinal barrier function. These findings pave the way for potential applications in treating and preventing colitis.

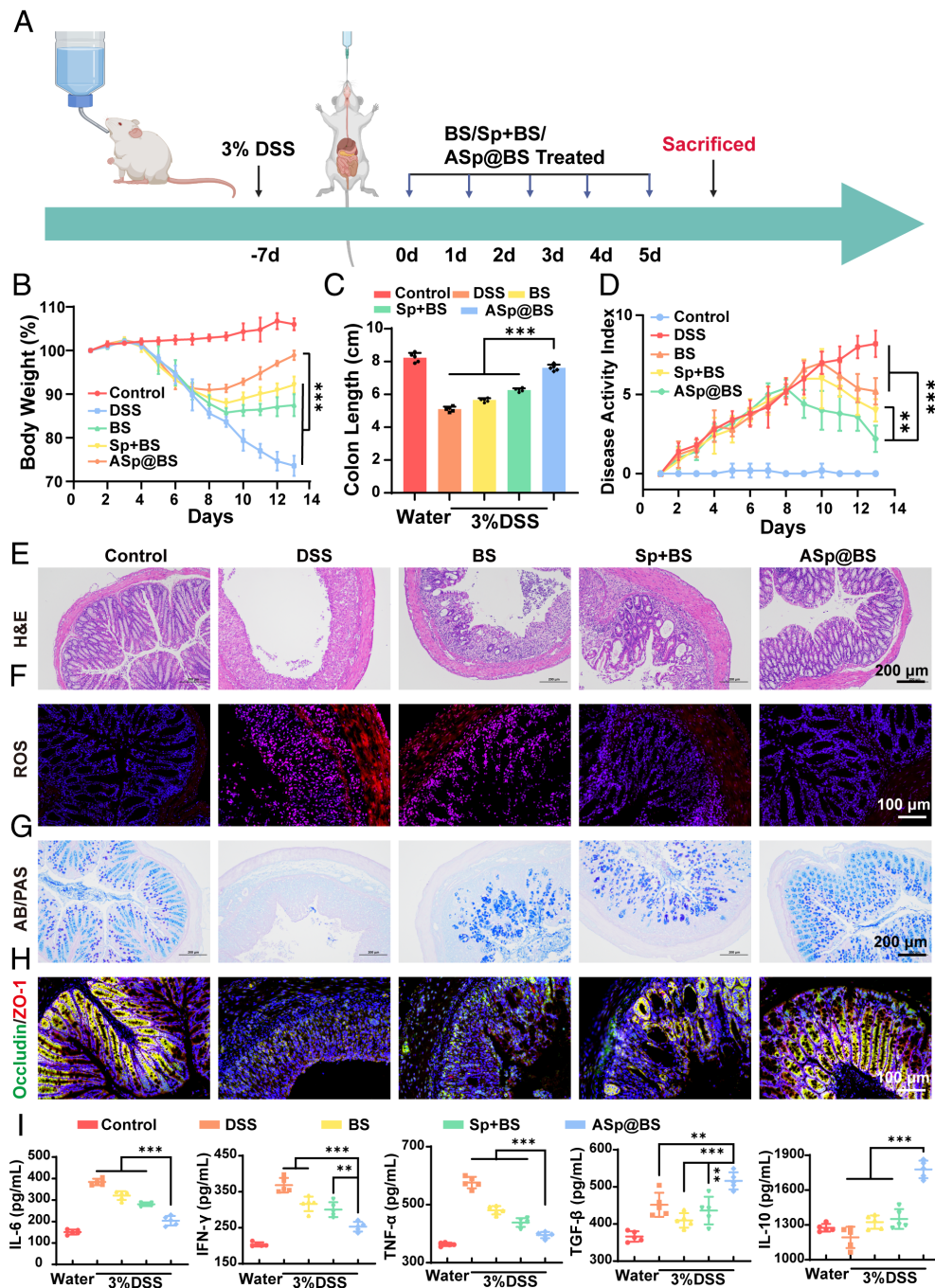


**Fig. 5.** ASp@BS ameliorated DSS-induced colitis. (A) C57BL/6 mice were provided water or 3% DSS-containing water for 7 d and orally administered medium, BS, Sp+BS, and ASp@BS. (B) Daily body-weight changes in each group were monitored for 13 d. Data were normalized as a percentage of the body weight at day 0. (C) Colon lengths of mice that received indicated treatments on day 13. (D) Changes in DAI for 13 d, which is the summation of the stool consistency index (0 to 3), fecal bleeding index (0 to 3), and weight loss index (0 to 4). (E) H&E staining of colonic sections of mice on day 13 after the indicated treatments. (Scale bar, 200  $\mu$ m.) (F) Representative ROS staining of colonic sections of colons of mice on day 13 after the indicated treatments. (Scale bar, 100  $\mu$ m.) (G) AB/PAS-staining of colonic sections of mice on day 13 after the indicated treatments. (Scale bar, 200  $\mu$ m.) (H) Immunofluorescence images of ZO-1 and occludin staining of the colon after the indicated treatments. (Scale bar, 100  $\mu$ m.) (I) Typical inflammatory cytokine levels of colons of mice on day 13 after the indicated treatments. Data are presented as the mean  $\pm$  SD ( $n = 5$ ); \* $P < 0.05$ , \*\* $P < 0.01$ , and \*\*\* $P < 0.001$ , determined by Student's *t* test.

### ASp@BS Regulates Colitis-Associated Gut Microbiota Dysbiosis.

Owing to the beneficial effects of probiotics in regulating gut microbiota, we examined the composition of the gut microbiota through 16S ribosomal RNA (rRNA) gene sequencing of the V3-V4 region. The Species Accumulation Boxplot indicated sufficient samples for subsequent analysis (Fig. 6A). The petal plot analysis revealed a total of 333 feature sequences across all groups, with 110, 38, 51, 32, and 108 unique feature sequences for Control, DSS, BS, Sp+BS, and ASp@BS, respectively (Fig. 6B). Principal

coordinates analysis (PCoA) was conducted to examine the  $\beta$ -diversity of the gut microbiota among the different treatment groups. The results showed that the gut microbiota composition of the ASp@BS treatment group was closest to that of the control group, indicating a positive shift toward healthier gut microbiota in response to ASp@BS treatment (Fig. 6C). Nonmetric multidimensional scaling was used to further assess the bacterial community structure. This analysis confirmed that ASp@BS treatment led to a significant shift of the bacterial community

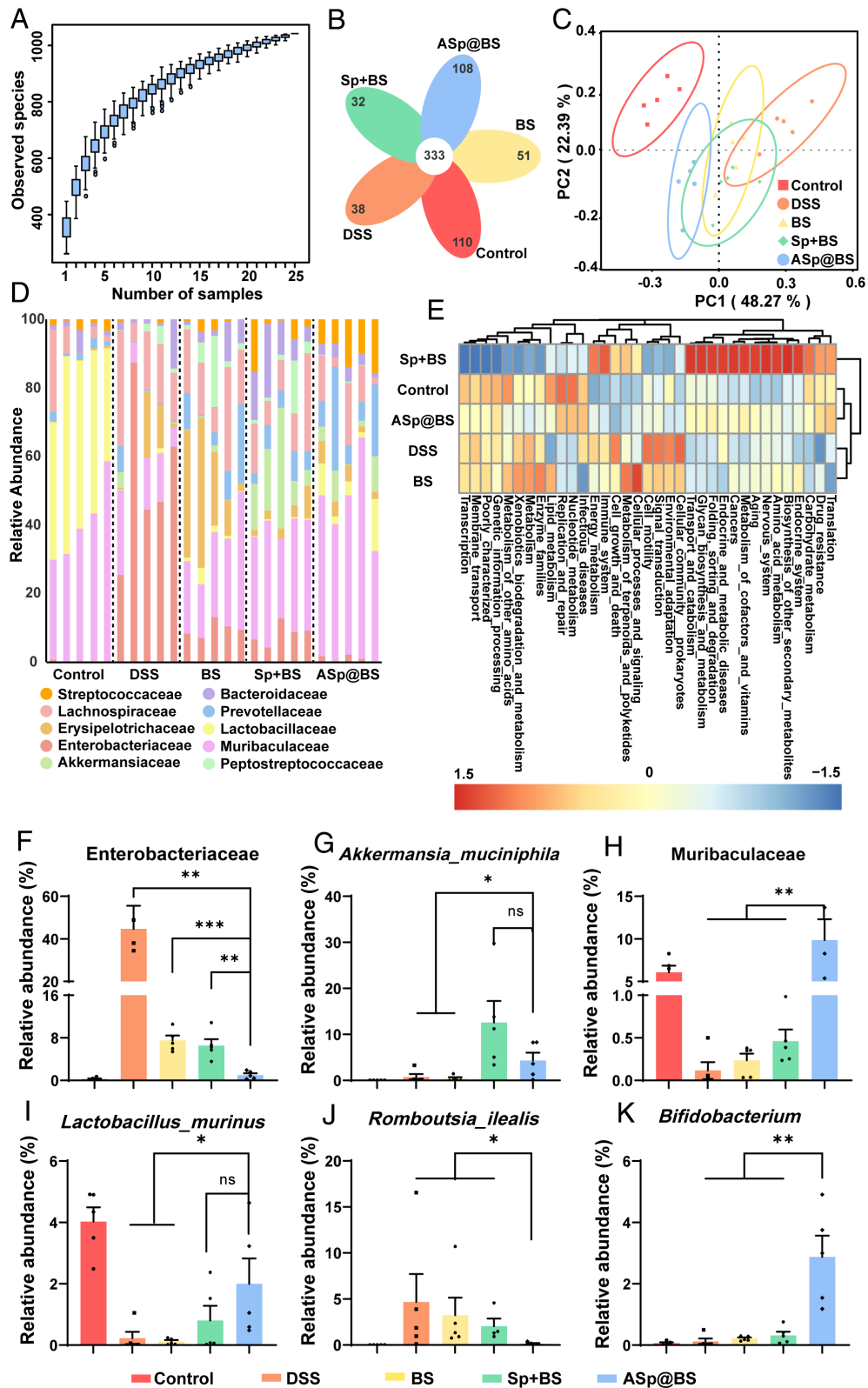


**Fig. 6.** ASp@BS regulates colitis-associated gut microbiota dysbiosis. (A) Box plots show the accumulation of alpha-diverse species in the gut microbiota. (B) Venn diagrams showing the differences in composition between different communities. (C) The PCoA plot shows the  $\beta$ -diversity of the intestinal microbiome ( $n = 5$ ). (D) Relative abundance of bacteria classified at the family-level taxonomic classification. (E) Dendrogram generated using the UPGMA method. (F–K) Relative abundance of selected taxa (F) *Enterobacteriaceae*, (G) *Akkermansia\_muciniphila*, (H) *Muribaculaceae*, (I) *Lactobacillus\_murinus*, (J) *Romboutsia\_ilealis*, and (K) *Bifidobacterium*. Data are presented as the mean  $\pm$  SD ( $n = 5$ ); \* $P < 0.05$ , \*\* $P < 0.01$ , and \*\*\* $P < 0.001$ , determined by Student's  $t$  test.

structure in untreated colitis mice closer to that of normal mice (SI Appendix, Fig. S23). Family-level species abundance bar plots were used to visualize the species composition in each treatment group. The results indicated that the gut microbiota composition

of the ASp@BS group was more similar to that of the control group than to other treatment groups, suggesting a favorable shift toward a healthier microbial composition (Fig. 6D). Additionally, based on functional annotations and abundance information of samples

in the database, we selected the top 35 abundant functions and their abundance information in each sample to create a heatmap. As depicted in Fig. 6E, the ASp@BS group clustered together with the normal control group, indicating a similar functional composition of the samples.

The bacterial composition of each treatment group was then analyzed in detail (Fig. 6 F–K). ASp@BS treatment significantly increased the relative abundance of *Akkermansia muciniphila* (known to be associated with protective intestinal barrier function) (43, 44), Muribaculaceae (known to regulate inflammatory responses) (45), *Lactobacillus murinus* (known to be negatively correlated with the inflammatory state of IBD) (46), and Bifidobacterium [known to enhance regulatory T cell (Treg) function and metabolism] (47), while significantly decreasing in the DSS group. Additionally, ASp@BS reduced the relative abundance of Enterobacteriaceae, which can thrive in inflamed intestines (48, 49), and *Romboutsia ilealis*, which can enhance IBD-related inflammatory responses (50). To further explain the observed differences in microbial composition, linear discriminant analysis effect size analysis was performed. Consistent with the above results, in the colitis mice of the control group, the abundance of Firmicutes was significantly reduced, while IBD-associated Enterobacteriaceae and Proteobacteria were significantly enriched (SI Appendix, Fig. S24). However, following ASp@BS treatment, the relative abundance of these pathogens decreased, and beneficial families such as Muribaculaceae, Lactobacillaceae, and Bifidobacteriaceae were significantly enriched relative to other groups, confirming the trend of ASp@BS regulating ecological imbalance in the gut (SI Appendix, Figs. S25 and S26). Additionally, ASp@BS treatment also slightly elevated the relative abundance of *Streptococcaceae* and *Prevotellaceae* (proinflammatory commensal bacteria). Despite increased levels of *Streptococcaceae* and *Prevotellaceae*, the overall composition of the ASp@BS treatment group was more similar to that of the control group. *t* test and Simper (Similarity Percentage) analysis also supported the conclusion that ASp@BS treatment played a role in regulating the gut microbiota, restoring balance, and potentially contributing to improved gut homeostasis in DSS-induced colitis mice (SI Appendix, Figs. S27 and S28). In conclusion, the study highlighted that ASp@BS treatment had a multifaceted impact on the gut microbiota by influencing its composition, function, and overall balance. This demonstrated the potential of ASp@BS to regulate gut homeostasis in the context of colitis, impacting oxidative-reduction balance, immune responses, and gut microbiota.

## Discussion

Prompt alleviation of inflammation and the restoration of equilibrium within the gut microbiota are pivotal aspects of successful IBD treatment (4, 51). Regrettably, conventional therapeutic approaches, encompassing the use of corticosteroids and TNF antagonists, have frequently yielded suboptimal outcomes while potentially exposing patients to associated risks, ultimately compromising their overall quality of life augmenting their susceptibility to more severe pathologies such as colon cancer (52–54). In response to these challenges, here, we developed ASp@BS with unique anti-inflammatory and gut microbiota-restoring properties and demonstrated its therapeutic efficacy in a mouse model of acute colitis. Within this unique symbiotic system, BS plays a pivotal role by activating hydrogenases within the Sp, thereby facilitating the generation of H<sub>2</sub>. The H<sub>2</sub> gas thus produced replaces conventional anti-inflammatory drugs, offering a distinct advantage owing to its capacity to efficiently neutralize ROS and subsequently mitigate inflammation. Importantly, this mechanism

underscores the biological safety of ASp@BS, setting it apart from conventional drug-based therapies. Furthermore, H<sub>2</sub> produced by Sp persistently eliminates ROS, exerting a powerful protective effect on the probiotics against oxidative damage under these inflammatory conditions. This synergy not only enhances bacterial survival but also expedites the restoration of intestinal barrier function and rectification of the disrupted gut microbiota, as depicted in Figs. 5 and 6, highlighting the profound therapeutic potential of ASp@BS.

We also observed a significant reduction in proinflammatory cytokines and ROS levels, concomitant with a substantial increase in anti-inflammatory factors, as shown in Fig. 5. Furthermore, ASp@BS treatment led to a notable upregulation in the expression of tight junction-related proteins within the colon. This dual action contributed to the simultaneous restoration of intestinal barrier function and protection of the epithelium from apoptotic processes, as illustrated in Fig. 5. Moreover, in a murine model of acute colitis induced by DSS, ASp@BS administration effectively facilitated the rapid recovery of lost body weight. Additionally, it exerted a suppressive effect on colonic and mucosal damage while significantly reducing colonic MPO activity. Intriguingly, these positive outcomes were not replicated in other control groups, including those administered BS+Sp and BS, highlighting the superior protective efficacy of ASp@BS in the context of colitis, as evident in Fig. 5. This phenomenon can be attributed to the ability of symbiotic aggregates to synergistically produce H<sub>2</sub> and modulate gut microbiota. BS could alleviate DSS-induced colitis by regulating the gut microbiota, promoting mucosal barrier reconstruction, and inhibiting the inflammatory response (29, 30). H<sub>2</sub> reprograms colonocyte metabolism by regulating the H<sub>2</sub>-gut microbiota-SCFA axis and strengthens the intestinal barrier by modulating specific mucosa-associated mucolytic bacteria, which, in turn, may alleviate colitis (35). Furthermore, the symbiotic interaction between Sp and BS enhances the therapeutic processes described. H<sub>2</sub> produced by Sp persistently eliminates ROS and protects probiotics from oxidative damage in the inflamed microenvironment. Although H<sub>2</sub> can remove hydroxyl radicals, it does not respond to H<sub>2</sub>O<sub>2</sub> in physiological conditions. Interestingly, we found that H<sub>2</sub> produced by Sp can be used by BS to defend against ROS. Specifically, the expression of antioxidant enzymes was increased after H<sub>2</sub> treatment (SI Appendix, Figs. S29 and S30). Coculture of Sp and BS enhances other aspects of the probiotics, which may contribute to the observed improvement in disease outcomes. This protection promotes the colonization and proliferation of BS, enhancing probiotic efficacy. Additionally, the extensive proliferation of BS consumes oxygen, creating an anaerobic environment that further stimulates H<sub>2</sub> production by Sp. These symbiotic effects collectively contribute to the promising therapeutic potential of ASp@BS against colitis. Crucially, in contrast to conventional immunosuppressive agents, which are associated with adverse events such as opportunistic infections, autoimmune reactions, and hepatotoxicity, our extensive investigation did not reveal any apparent toxicity related to repeated ASp@BS treatment, as evidenced in SI Appendix, Figs. S14 and S15. These compelling findings underscore the safety and efficacy of ASp@BS as a potential therapeutic approach for colitis.

The growing acknowledgment of the pivotal role played by the gut microbiota in human health has led to an increased understanding of its involvement in numerous human diseases, including IBD, obesity, diabetes, cancer, and neurological disorders (1, 8, 55). In this context, our ASp@BS treatment demonstrated the capacity to modulate the gut microbiota effectively. This modulation was characterized by an augmentation in the diversity and

relative abundance of beneficial probiotics, including, but not limited, to *Akkermansia muciniphila*, Muribaculaceae, *Lactobacillus murinus*, and *Bifidobacterium*, as illustrated in Fig. 6. Notably, ASp@BS also exerted a favorable influence by decreasing the relative abundance of potentially harmful Proteobacteria, particularly Enterobacteriaceae, which tend to thrive in the inflamed gut environment. Additionally, ASp@BS curtailed the presence of *Romboutsia ilealis*, known to exacerbate the inflammatory response in IBD. BS can secrete surface-active agents, plipastatin, or bacteriocin-like secondary metabolites, inhibiting the growth of harmful bacteria (29, 30). Additionally, BS can produce beneficial metabolites such as short-chain fatty acids (SCFAs), which have a positive impact on the gut microbiota (29, 30). The H<sub>2</sub>-producing properties of ASp@BS are also beneficial for the modulation of gut microbiota homeostasis. Previous research has shown that H<sub>2</sub> administration can increase the abundance of intestinal-specific SCFA-producing bacteria and therefore enhance SCFA production. H<sub>2</sub> also modulates specific mucosa-associated mucolytic bacteria, leading to substantial inhibition of the spread of opportunistically pathogenic *Escherichia coli* in mice with colitis (35). The reduction of ROS by ASp@BS also contributes to the regulation of gut microbiota. Studies have shown that ROS are detrimental to the growth of beneficial bacteria and can be utilized by facultative anaerobic pathogenic bacteria, leading to their proliferation (4, 34, 56). The research results highlight the ability of the ASp@BS system to enhance probiotic activity, increase H<sub>2</sub> generation, and reduce ROS, ultimately enabling the modulation of gut microbiota homeostasis. Collectively, these findings emphasize the multifaceted benefits of ASp@BS, which extend beyond its protective effects on the colonic epithelium against inflammation to restoration of disrupted gut microbiota and intestinal barrier function. Given the well-established link between dysregulated gut microbiota and compromised intestinal barrier function in systemic diseases, the approach delineated herein holds promise as a versatile and potent platform for the treatment of various inflammatory conditions.

1. Y. Lee *et al.*, Hyaluronic acid-bilirubin nanomedicine for targeted modulation of dysregulated intestinal barrier, microbiome and immune responses in colitis. *Nat. Mater.* **19**, 118–126 (2020).
2. B. M. Scott *et al.*, Self-tunable engineered yeast probiotics for the treatment of inflammatory bowel disease. *Nat. Med.* **27**, 1212–1222 (2021).
3. Q.-X. Huang *et al.*, Stimulation-responsive mucoadhesive probiotics for inflammatory bowel disease treatment by scavenging reactive oxygen species and regulating gut microbiota. *Biomaterials* **301**, 122274 (2023).
4. F. Cao *et al.*, Artificial-enzymes-armed Bifidobacterium longum probiotics for alleviating intestinal inflammation and microbiota dysbiosis. *Nat. Nanotechnol.* **18**, 617–627 (2023).
5. D. van der Lelie *et al.*, Rationally designed bacterial consortia to treat chronic immune-mediated colitis and restore intestinal homeostasis. *Nat. Commun.* **12**, 3105 (2021).
6. J. Zhou *et al.*, Programmable probiotics modulate inflammation and gut microbiota for inflammatory bowel disease treatment after effective oral delivery. *Nat. Commun.* **13**, 3432 (2022).
7. Q. Zhang *et al.*, A superoxide dismutase/catalase mimetic nanomedicine for targeted therapy of inflammatory bowel disease. *Biomaterials* **105**, 206–221 (2016).
8. C. Li *et al.*, A Proresolving peptide nanotherapy for site-specific treatment of inflammatory bowel disease by regulating proinflammatory microenvironment and gut microbiota. *Adv. Sci.* **6**, 1900610 (2019).
9. C. Zhang *et al.*, Oral colon-targeted mucoadhesive micelles with enzyme-responsive controlled release of curcumin for ulcerative colitis therapy. *Chinese Chem. Lett.* **33**, 4924–4929 (2022).
10. M. E. Sanders, D. J. Merenstein, G. Reid, G. R. Gibson, R. A. Rastall, Probiotics and prebiotics in intestinal health and disease: From biology to the clinic. *Nat. Rev. Gastroenterol. Hepatol.* **16**, 605–616 (2019).
11. L. Y. Wan, Z. J. Chen, N. P. Shah, H. El-Nezami, Modulation of intestinal epithelial defense responses by probiotic bacteria. *Crit. Rev. Food Sci. Nutr.* **56**, 2628–2641 (2016).
12. T. J. Ashaolu, Immune boosting functional foods and their mechanisms: A critical evaluation of probiotics and prebiotics. *Biomed. Pharmacother.* **130**, 110625 (2020).
13. J. Li *et al.*, Polydopamine nanoparticle-mediated dopaminergic immunoregulation in Colitis. *Adv. Sci.* **9**, e2104006 (2022).
14. X. Kuang *et al.*, Triggerable prodrug nanocoating enables on-demand activation of microbial and small-molecular therapeutics for combination treatment. *J. Am. Chem. Soc.* **145**, 26932–26946 (2023).
15. H. Luo *et al.*, Chemical reaction-mediated covalent localization of bacteria. *Nat. Commun.* **13**, 7808 (2022).
16. X. Yang *et al.*, Physiologically inspired mucin coated *Escherichia coli* Nissle 1917 enhances biotherapy by regulating the pathological microenvironment to improve intestinal colonization. *ACS Nano* **16**, 4041–4058 (2022).

## Materials and Methods

See *SI Appendix, Materials and Methods* for technical details for each method.

**Preparation and Characterization of ASp@BS.** ASp@BS was synthesized using a biomimetic silica mineralization method and subsequently characterized by various techniques, including CLSM, EDS, Fourier-transform infrared spectroscopy (FT-IR), and DLS.

**In Vitro Characterization of ASp@BS.** The H<sub>2</sub> production capability of ASp@BS was assessed using gas chromatograph and a Methylene Blue-Platinum (MB-Pt) probe. The survival of bacterial cells was evaluated through colony counting methods.

**In Vivo Characterization of ASp@BS.** All experiments adhered to international guidelines. Animal studies were conducted following protocols reviewed and approved by the Institutional Animal Care and Use Committee of Zhengzhou University. The in vivo distribution of ASp@BS was examined using in vivo imaging techniques. The biosafety of ASp@BS was assessed in healthy mice. The therapeutic efficacy of ASp@BS was evaluated in mice with DSS-induced colitis.

**Data, Materials, and Software Availability.** All study data are included in the article and/or *SI Appendix*. Bacterial V4–16S rRNA amplicon sequencing data in raw format prior to postprocessing and data analyses have been deposited at the NCBI SRA, under accession no. [PRJNA1187480](https://doi.org/10.1093/bioinformatics/btad057) (57). RNA-seq data for *Bacillus subtilis* have been deposited at the NCBI SRA, under accession no. [PRJNA1187674](https://doi.org/10.1093/bioinformatics/btad058) (58).

**ACKNOWLEDGMENTS.** This work was supported by the National Natural Science Foundation of China [Nos. 82222067, 82172762, 82373287, 21904119, and 82073395]; Outstanding Youth Foundation of Henan Province (No. 222300420020); Key Projects of Advantageous Disciplines in Henan Province (No. 222301420011); Science and Technology Innovation Talents Support Project of Henan Province (No. 23HASTIT041); Henan Provincial Science and Technology Research and Development Plan Joint Fund (No. 222301420050); and Henan Science Fund for Outstanding Young Scholars (No. 232300421051). We would like to express our gratitude to the Shijianjia Lab ([www.shijianjia.com](http://www.shijianjia.com)) for the ICP-MS.

17. J. Yang *et al.*, An oral "Super probiotics" with versatile self-assembly adventitia for enhanced intestinal colonization by autonomously regulating the pathological microenvironment. *Chem. Eng. J.* **446**, 137204 (2022).
18. D. Wei, Y. Sun, H. Zhu, Q. Fu, Stimuli-responsive polymer-based nanosystems for cancer theranostics. *ACS Nano* **17**, 23223–23261 (2023).
19. S. D. Veresoglou, D. Johnson, Species-area relationships in microbial-mediated mutualisms. *Trends Microbiol.* **31**, 1111–1117 (2023).
20. D.-W. Zheng *et al.*, An orally delivered microbial cocktail for the removal of nitrogenous metabolic waste in animal models of kidney failure. *Nat. Biomed. Eng.* **4**, 853–862 (2020).
21. D.-W. Zheng *et al.*, Prebiotics-encapsulated probiotic spores regulate gut microbiota and suppress colon cancer. *Adv. Mater.* **32**, e2004529 (2020).
22. Y. Zhang *et al.*, Double bacteria synergistic catalytic reduction system for heavy metal detoxification treatment. *Nano Lett.* **22**, 5575–5583 (2022).
23. J.-Y. Qiao *et al.*, Autonomously assembled living capsules by microbial coculture for enhanced bacteriotherapy of inflammatory bowel disease. *Nano Lett.* **23**, 4375–4383 (2023).
24. E. Touloupakis *et al.*, Hydrogen production by immobilized *Synechocystis* sp. PCC 6803. *Int. J. Hydrogen Energy* **41**, 15181–15186 (2016).
25. Y. Wang *et al.*, Microalgal hydrogen production. *Small Methods* **4**, 1900514 (2020).
26. E. Touloupakis, A. M. S. Benavides, B. Cicchi, G. Torzillo, Growth and hydrogen production of outdoor cultures of *Synechocystis* PCC 6803. *Algal Res.* **18**, 78–85 (2016).
27. L. J. Rios-González *et al.*, Potential of *Bacillus subtilis* as oxygen-removal agent for biohydrogen production by *Clostridium acetobutylicum*. *Int. J. Hydrogen Energy* **49**, 572–576 (2023).
28. Y. Liu *et al.*, Long-term and continuous administration of *Bacillus subtilis* during remission effectively maintains the remission of inflammatory bowel disease by protecting intestinal integrity, regulating epithelial proliferation, and reshaping microbial structure and function. *Food Funct.* **12**, 2201–2210 (2021).
29. Q. Hou *et al.*, *Bacillus subtilis* programs the differentiation of intestinal secretory lineages to inhibit *Salmonella* infection. *Cell Rep.* **40**, 111416 (2022).
30. Á. T. Kovács, *Bacillus subtilis*. *Trends Microbiol.* **27**, 724–725 (2019).
31. Y. Litvak, M. X. Byndloss, A. J. Bäuml, Colonocyte metabolism shapes the gut microbiota. *Science* **362**, eaat9076 (2018).
32. P. Luo, H. Wang, X. Wen, X. Luo, P. Xu, Unveiling the multifunction of beaded stream-like Co9Se8 catalysts for water splitting, reactive oxygen species scavenging, and hydrogen anti-inflammation. *Adv. Mater.* **14**, 2302532 (2024).
33. Y. You *et al.*, Water-enabled H<sub>2</sub> generation from hydrogenated silicon nanosheets for efficient anti-inflammation. *J. Am. Chem. Soc.* **144**, 14195–14206 (2022).

34. J. Liu *et al.*, Mucoadhesive probiotic backpacks with ROS nanoscavengers enhance the bacteriotherapy for inflammatory bowel diseases. *Sci. Adv.* **8**, eabp8798 (2022).
35. L. Ge *et al.*, Microbial hydrogen economy alleviates colitis by reprogramming colonocyte metabolism and reinforcing intestinal barrier. *Gut Microbes* **14**, 2013764 (2022).
36. Y.-X. Zhu *et al.*, Inorganic nanosheet-shielded probiotics: A self-adaptable oral delivery system for intestinal disease treatment. *Nano Lett.* **23**, 4683–4692 (2023).
37. Y. Song *et al.*, Micromotor-enabled active hydrogen and tobramycin delivery for synergistic sepsis therapy. *Adv. Sci.* **10**, e2303759 (2023).
38. F. Gong *et al.*, Nanoscale CaH<sub>2</sub> materials for synergistic hydrogen-immune cancer therapy. *Chem* **8**, 268–286 (2022).
39. W. Xiong *et al.*, Silicification-induced cell aggregation for the sustainable production of H<sub>2</sub> under aerobic conditions. *Angew. Chem. Int. Ed. Engl.* **54**, 11961–11965 (2015).
40. S. H. Yang *et al.*, Biomimetic encapsulation of individual cells with silica. *Angew. Chem. Int. Ed. Engl.* **48**, 9160–9163 (2009).
41. W. Xiong *et al.*, Prevention of cyanobacterial blooms using nanosilica: A biomineralization-inspired strategy. *Environ. Sci. Technol.* **51**, 12717–12726 (2017).
42. D. Wei *et al.*, Nuclear-targeting lipid Pt(IV) prodrug amphiphile cooperates with siRNA for enhanced cancer immunotherapy by amplifying Pt-DNA adducts and reducing phosphatidylserine exposure. *J. Am. Chem. Soc.* **146**, 1185–1195 (2024).
43. P. D. Cani, W. M. de Vos, Next-generation beneficial microbes: The case of *Akkermansia muciniphila*. *Front. Microbiol.* **8**, 1765 (2017).
44. Z. Zhang *et al.*, Chlorogenic acid ameliorates experimental colitis by promoting growth of *Akkermansia* in mice. *Nutrients* **9**, 677 (2017).
45. L. Shang *et al.*, Core altered microorganisms in colitis mouse model: A comprehensive time-point and fecal microbiota transplantation analysis. *Antibiotics (Basel)* **10**, 643 (2021).
46. N. Tang *et al.*, Extraction, isolation, structural characterization and prebiotic activity of cell wall polysaccharide from *Kluyveromyces marxianus*. *Carbohydr. Polym.* **289**, 119457 (2022).
47. K. Wang *et al.*, Mucoadhesive probiotic-based oral microcarriers with prolonged intestinal retention for inflammatory bowel disease therapy. *Nano Today* **50**, 101876 (2023).
48. J. Yang *et al.*, Bionic regulators break the ecological niche of pathogenic bacteria for modulating dysregulated microbiome in colitis. *Adv. Mater.* **34**, e2204650 (2022).
49. W. Zhu *et al.*, Precision editing of the gut microbiota ameliorates colitis. *Nature* **553**, 208–211 (2018).
50. A. Santiago *et al.*, Crohn's disease proteolytic microbiota enhances inflammation through PAR2 pathway in gnotobiotic mice. *Gut Microbes* **15**, 2205425 (2023).
51. Y. Zeng *et al.*, Reactive oxygen species-activated CO versatile nanomedicine with innate gut immune and microbiome remodeling effects for treating inflammatory bowel disease. *Adv. Funct. Mater.* **33**, 2304381 (2023).
52. H. Liu *et al.*, Colon-targeted adhesive hydrogel microsphere for regulation of gut immunity and flora. *Adv. Sci.* **8**, e2101619 (2021).
53. J. P. Gisbert, A. C. Marin, M. Chaparro, The risk of relapse after anti-TNF discontinuation in inflammatory bowel disease: Systematic review and meta-analysis. *Am. J. Gastroenterol.* **111**, 632–647 (2016).
54. M. T. Abreu, Combining biologic agents in inflammatory bowel disease. *Gastroenterol. Hepatol. (NY)* **15**, 549–551 (2019).
55. S. Liu, W. Zhao, P. Lan, X. Mou, The microbiome in inflammatory bowel diseases: From pathogenesis to therapy. *Protein Cell* **12**, 331–345 (2021).
56. Q. Ren, S. Sun, X.-D. Zhang, Redox-active nanoparticles for inflammatory bowel disease. *Nano Res.* **14**, 2535–2557 (2021).
57. J. Yang *et al.*, Bacterial V4–16S rRNA amplicon sequencing data. NCBI. <https://www.ncbi.nlm.nih.gov/bioproject/?term=PRJNA1187480>. Deposited 18 November 2024.
58. Z.-H. Wang *et al.*, RNA-seq data for *Bacillus subtilis*. <https://www.ncbi.nlm.nih.gov/sra/?term=PRJNA1187674>. Deposited 18 November 2024.